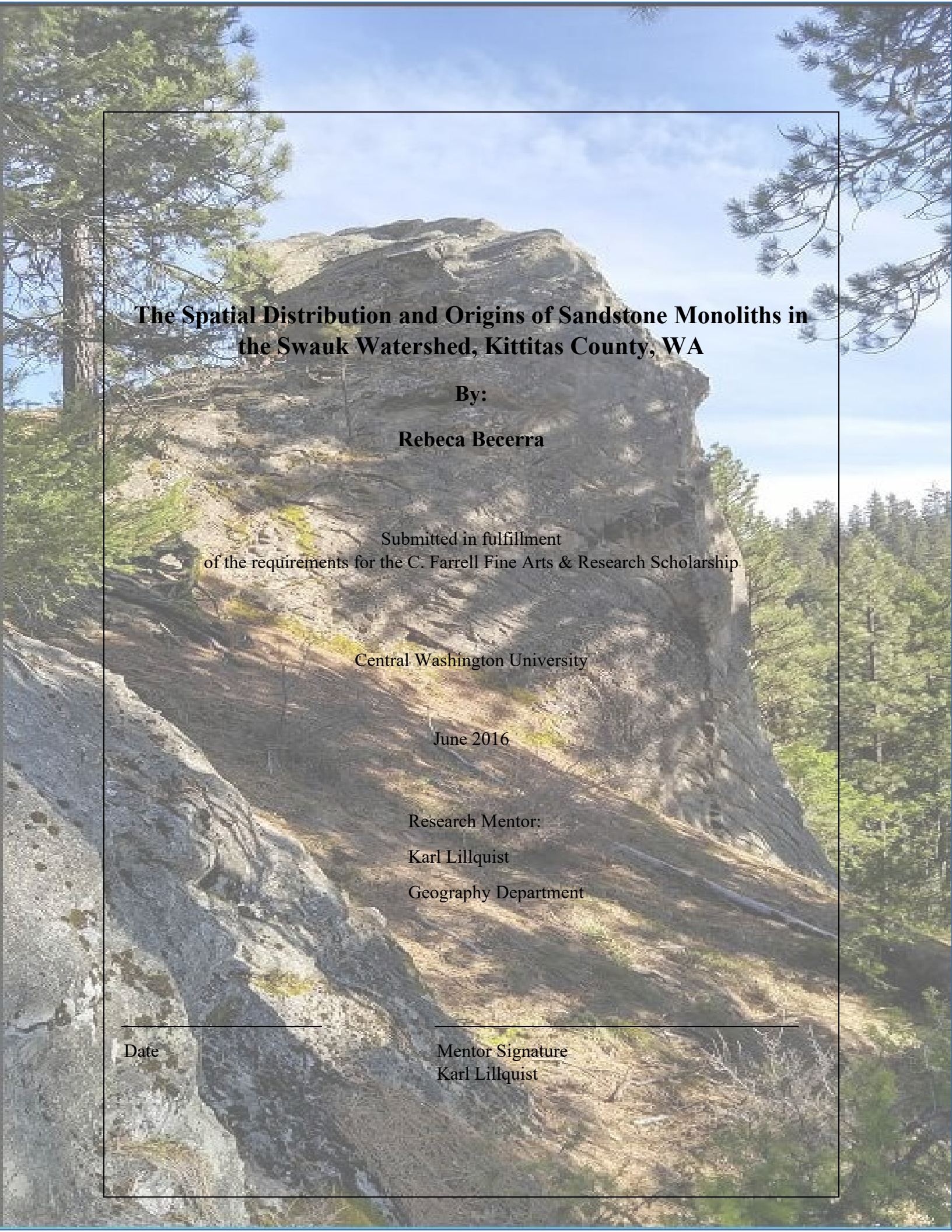

# The Spatial Distribution and Origins of Sandstone Monoliths in the Swauk Watershed, Kittitas County, WA


**By:**

**Rebeca Becerra**


Submitted in fulfillment
of the requirements for the C. Farrell Fine Arts & Research Scholarship

Central Washington University

June 2016

Research Mentor:

Karl Lillquist

Geography Department

_____

Date

_____

Mentor Signature
Karl Lillquist

**Abstract**: Large groups of gigantic sandstone and conglomerate monoliths populate the Swauk Watershed of northern Kittitas County. These monoliths rest on side slopes in the watershed and distinctively project from their surroundings. The origins of these features are unknown. We studied these monoliths in the field by mapping their spatial distribution, describing their morphology and composition, and measuring their orientation and sizes in order to determine their origins. We used Google Earth and topographic maps to locate the monoliths and map their distribution. Interpretations were based from field work data and past research. Our field results show commonalities between the features related to overall structure, composition, and geomorphology. All monoliths studied are associated with dipping strata. Dip slopes are gently sloping while anti-dip slopes are much steeper. The monoliths also have distinct and traceable conglomerate layers that are highly resistant to erosion, as well as thick sandstone layers and some smaller pebble layers. These features also share similar geomorphology: they are surrounded by channels; fresh surfaces are lichen-free; honeycomb weathering and overhangs dominate the anti-dip slopes; and prominent vertically aligned jointing parallels the dipping beds. The strike and dip measurements of the monoliths are aligned with the crests and troughs of synclines and anticlines shown on the geologic map of the area. These results indicate that geologic composition and structure play a significant role in the initial shaping of these landforms. Differential weathering, fluvial erosion, and mass movement have together weakened the sandstone, causing backwasting of low bedrock escarpments and the carving out of vertically aligned joints. The repetitive cycle of weathering, mass movement, and stream erosion has ultimately been the cause of the isolation of the sandstone monoliths over time.

**Introduction**:

*Problem.* The Swauk Watershed lies in a structural basin between the Straight Creek and Entiat-Leavenworth fault systems in northern Kittitas County in the Eastern Cascades of Washington state. Swauk Formation deposition began 59.9 million years ago (Ma), when west to southwest flowing streams laid down sands and gravels (Eddy et al., 2015) that were later lithified. Tectonic uplift and folding followed, thereby complicating the geology. These sediments were intruded by Teanaway dikes 47 Ma, after folding occurred (Miller, 2014).

Throughout the Swauk Watershed lie numerous, noticeably tilted "monoliths" composed of sandstone & conglomerate. These monoliths rest on side slopes in the watershed and distinctively project from their surroundings. Similar features have been found elsewhere. In the Carpathian Mountains of Poland, these remnants have been defined as products of subsurface water erosion and selective weathering (Alexandrowicz and Urban, 2005). In Somerset Island, Canada, similar features are defined as residuals of differential weathering and mass movement (Dyke, 1976). Such monoliths have been discussed in the literature as *tors*. The definition of a tor is an individual rocky form separated from the slope and other landforms and characterized by walls sculpted by weathering processes. They are predominantly located in the upper parts of mountain ranges (Alexandrowicz and Urban, 2005). Could the Swauk Watershed monoliths be tors? Are their origins tied to differential weathering and mass movement, like Dyke (1976) proposes, or more along the lines of fluvial erosion and weathering, as Alexandrowicz and Urban (2005) proposes? Could they have formed from a combination of all of the above processes?

*Purpose.* The intent of researching the monoliths of the Swauk Watershed was to: (1) map the spatial distribution of these landforms; (2) describe the morphology and identify the compositions of these features; and (3) determine their origins.

*Significance.* These monoliths should ultimately reveal clues about the geomorphic development and evolution of the Swauk Watershed. The same processes that have impacted mass wasting in the Swauk Watershed could be the same processes that have triggered, and continue to trigger, the

development of the monoliths. Active mass wasting is triggered by precipitation and snowmelt derived primarily from rain-on-snow events, and occurs where slopes have been steepened by road-cuts and stream cuts and where vegetation has been removed by logging (Lillquist, 2001). My research in the Swauk Watershed could offer support for the idea that headward recession and pore water infiltration has been active in the area. My research on the Swauk Watershed monoliths can also provide some further insight on the timing of mass wasting in the watershed. Others may then apply my findings to similar surrounding basins (e.g. Peshastin Creek and the Teanaway River watersheds) to help better understand the geomorphic history of the region. Finally, my work on sandstone monoliths can also help us better understand the geomorphology of continental sandstone environments in terms of lithological variation and geological structures as well as the chemical weathering and erosional processes that are involved in creating these features.

**Study Area Description**:

The Swauk basin is a structural (i.e. fault-bounded) sedimentary basin that was once a broadly subsiding coastal plain (Evans, 1994) that rests on the southern flanks of the crystalline Cascades core of the North Cascades (Miller, 2014). It is one of the several Eocene nonmarine basins in western and central Washington that formed within a regional network of right-lateral, strike-slip faults (Johnson, 1985). The Swauk Watershed lies in the Swauk basin in the Eastern Cascades of Washington state, in northern Kittitas County (Fig. 1). The watershed is a mountainous region bordered by Blewett Pass to the north, Teanaway Ridge to the west, and Table Mountain to the east. The watershed is a north-south trending basin that ranges in elevation from 600-1800 m, annual precipitation ranges from 20” to 40”, with heavier precipitation being the norm the further north one travels (Erickson, 2001). Local climate is influenced by the Cascade Mountains, by deep, steep-sloped valleys, and by prevailing westerly winds (Camp, 1999). Precipitation declines along a steep west to east gradient, and occurs during late fall and winter, with much of it in the form of snow (Camp, 1999). The Swauk Watershed vegetation includes a mosaic of ponderosa pine, Douglas-fir and grand fir, moist grand fir, mesic Douglas-fir and subalpine fir, all controlled by the geology, weather patterns, and soils (Stephenson, 1997).

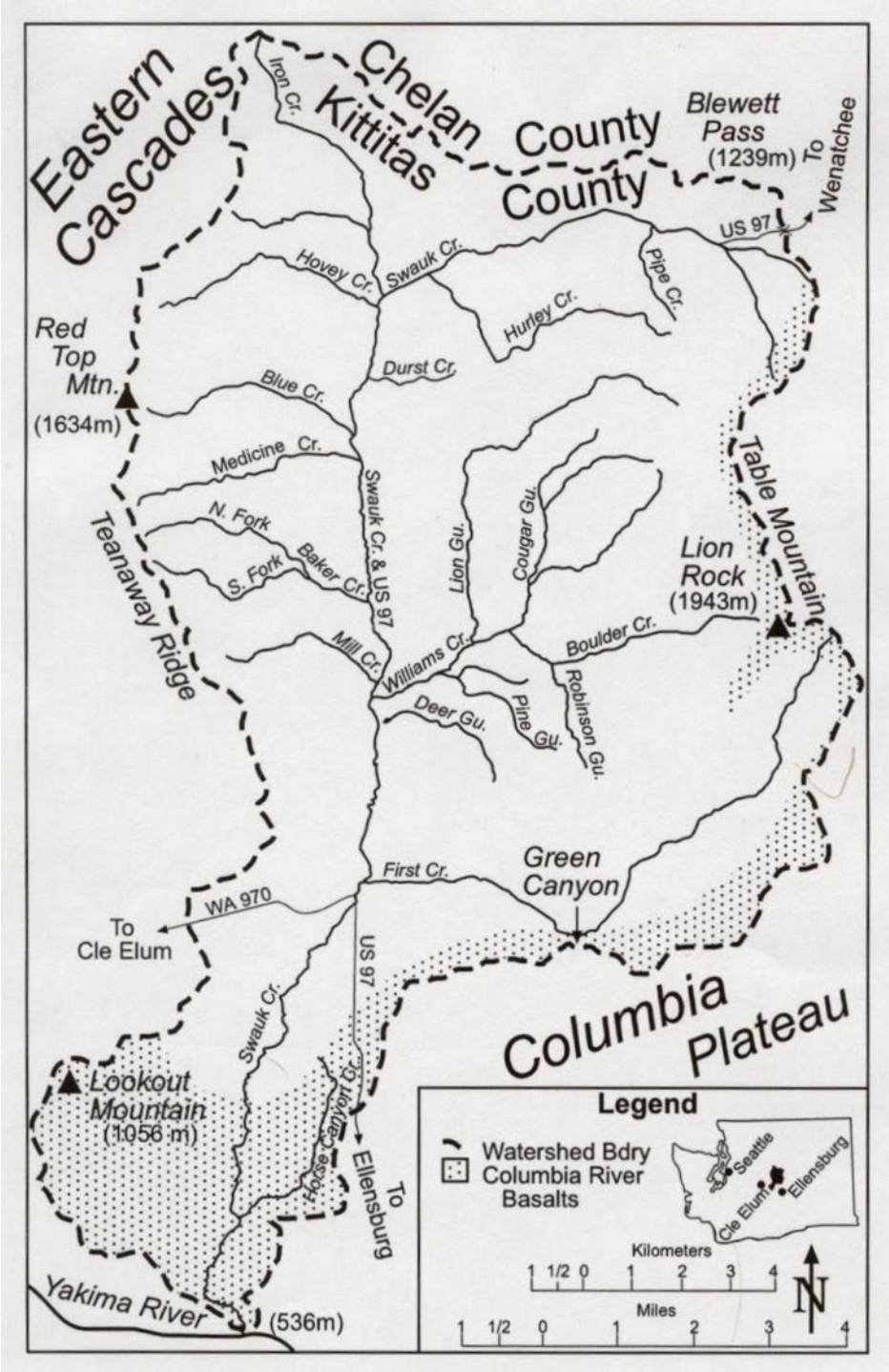


**Fig. 1.** The Swauk Watershed boundary (Lillquist, 2001).

Current vegetation structures and patterns within the Swauk drainage have been influenced by human occupation and management (Stephenson, 1997). Some notable stream valleys of the watershed that cross my field area include Hurley Creek, Durst Creek, Williams Creek, Swauk Creek, Lion Gulch, Cougar Gulch, and Billy Goat Gulch.

**Methods**:

*Pre-field.* Before going to the field area to collect data, assistant Daniel O'Dell and I began mapping the monoliths on Google Earth and with a topographic map. In Google Earth, the monoliths showed up as bright white-grey spots against the green background of the trees (Fig. 2). This is due to the monoliths being mostly made up of white to tan sandstone, which made them easy to identify. On the topographic map, it was harder to discern the monoliths because they were not always distinguished with the contours (Fig. 3). This made Google Earth my primary source for finding the monoliths and the topographic maps for use in the field while driving around with no cell service. After mapping at least 3 monoliths for the coming field day, we created a data sheet to use in the field so we wouldn't forget to collect any data. The data sheet includes all the collectable data that now makes up the data table in the


**Fig. 2.** Google Earth image of CT1 and CT2.


**Fig. 3.** Image of the topo map with monoliths marked (U.S. Geological Survey Liberty, WA 7.5' Quadrangle).

results section. Each week before the next field day, we would update Google Earth and the topographic maps with new monoliths and new routes that we found from Google Earth.

*In the field.* After mapping the monoliths onto a topographic map, assistant Daniel O'Dell and I conducted field work on 6 Saturdays through Spring 2016. Data collection began with naming each feature (e.g. "CG1," "LR1" based on something notable about the area or monolith), taking a GPS waypoint, recording the elevation of the monolith's highest point, and walking around the monolith to get a rough measurement of circumference with the LG Health app (to cross-reference with dimensions given by Google Earth later) and also to become accustomed to the feature. This step also allowed us to take strike and dip measurements with our Brunton pocket transits in multiple places where bedding was well defined. Afterwards, we took a closer look at weathering features such as honeycombs, potholes, sheeting structures, and the presence of grüs around the feature. We checked lichen coverage on all sides (including the top of the feature) and estimated its percent coverage with a modal abundance chart. Before obtaining trend and plunge measurements of joints, we first determined if they were actually joints or just sheets of exfoliation. To determine this, we used the thickness of the outermost layer-- exfoliation tends to

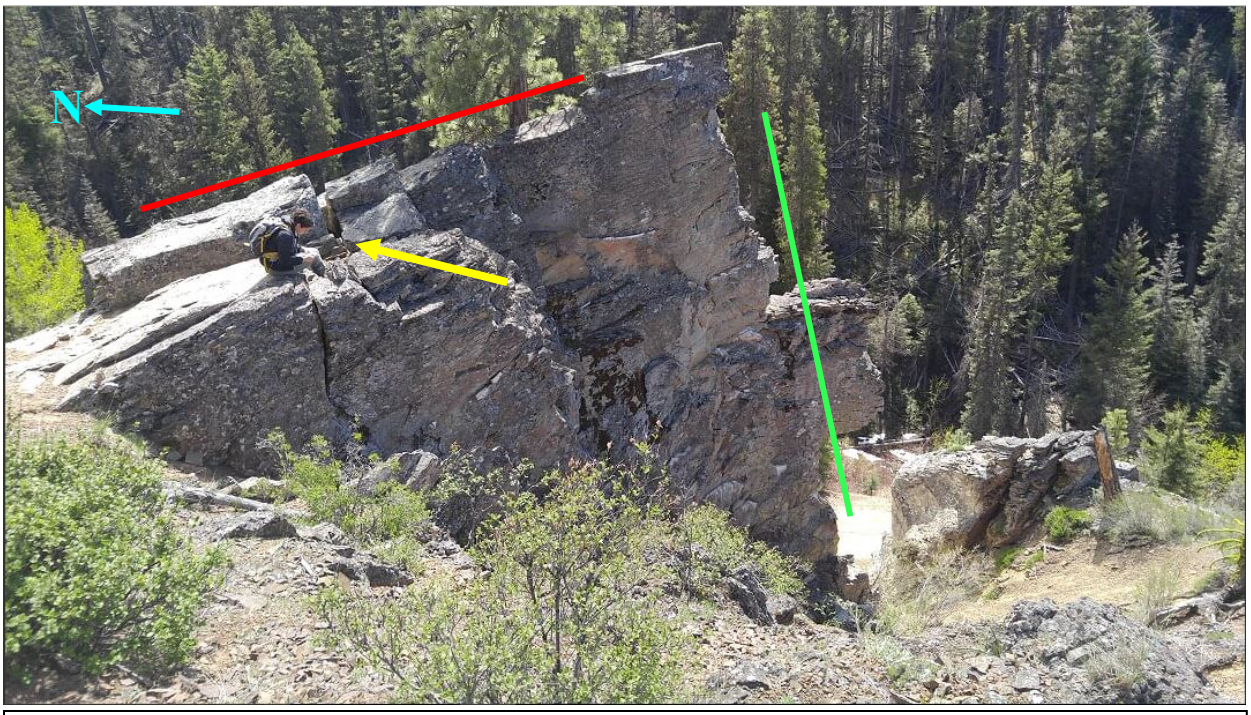


**Figure 4.** Anti-dip (Green) and dip slope (Red) of monolith at site HC1 (Fig. 10 shows location of this site). Myself taking trend and plunge measurements for scale (Yellow arrow). View SW. Daniel O'Dell photo.

be a thin sheet-like feature, whereas joints are larger and continue throughout the entire monolith. To take trend and plunge, we lined up the Brunton pocket transit parallel to the joint to get an orientation, and then measured the incline of the joints from horizontal. Along with taking trend and plunge measurements, we also recorded the aspect of the joints with a Brunton pocket transit. We also took aspect measurements of the anti-dip slopes that were found on the monoliths. Anti-dip slopes are characterized by a steep cliff that abruptly drops off (Fig. 4). When we reached the lowest point of the monolith, we used a Leopold laser rangefinder capable of viewing distances as far as 20 km to measure the distance from our point to the top of the monolith and the angle of that point from the ground. Both values were used later to calculate monolith heights using the Pythagorean Theorem. Other measurements we made included bedding thicknesses of the sandstone and conglomerate, the sizes and aspects of cannonballs (i.e., cannonball-shaped masses that were embedded into the sandstone) (Figs. 5, 6, and 7), and the sizes of the monolith overhangs (i.e., rounded blocks or sheets of sandstone hanging over the monolith) (Figs. 8 and 9).

**Figure 5.** Cannonball-shaped mass (white arrow) at site HC2 (see Fig. 10 for location). NW face of monolith. Nearby tree for scale (30 ft tall). Daniel O'Dell photo.

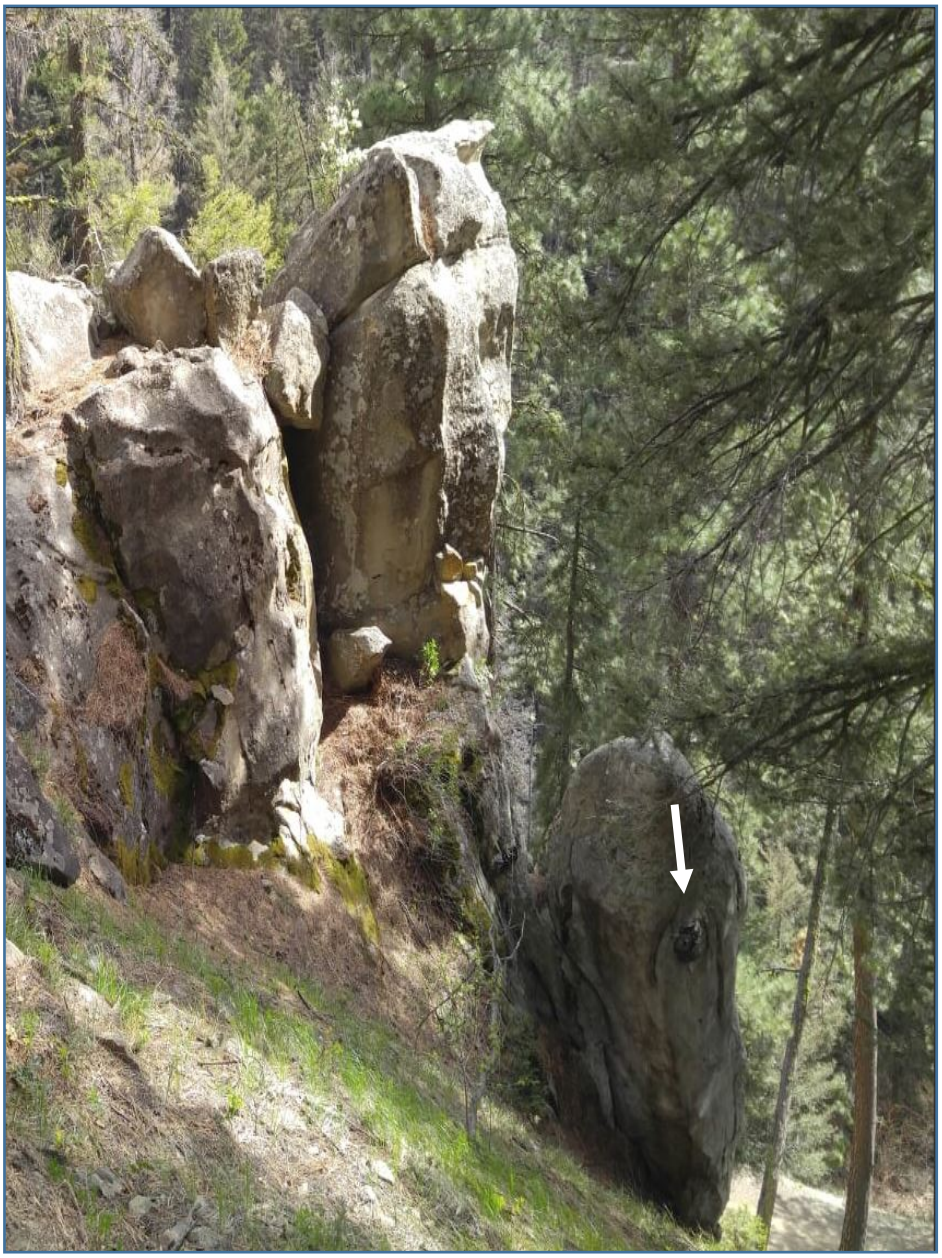

**Figure 6.** Large Cannonball (white arrow) at site HC2 on rounded pillar. SE side of monolith. Tree for scale (100 ft tall). Daniel O'Dell photo.

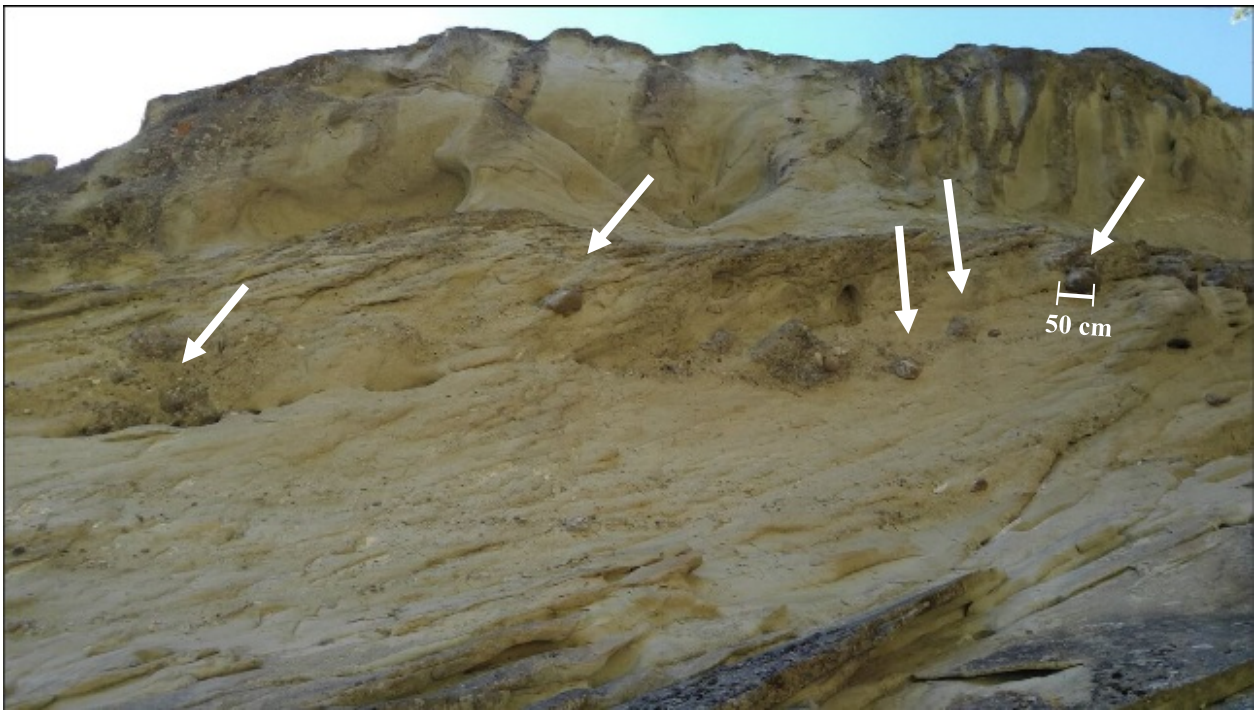


**Figure 7.** Cannonballs (white arrows) lining the E face of site CT2. Note how they are embedded in the sandstone. Largest cannonball was 50 cm across. Daniel O'Dell photo.

**Figure 8.** Sheet-like overhangs (black arrows) created by jointing on the NW face of site CG2. Tree on the right is 100 ft tall. Daniel O'Dell photo.

**Figure 9.** Tilted overhang on top of site CT1 (yellow). N face. Tree is 2 m tall (blue). Daniel O'Dell photo.

*Post field.* After field work, assistant Daniel O'Dell and I input newly retrieved data into a data table and mapped monoliths to visit in the future onto Google Earth and on my topo map. I cross-referenced my circumference data with dimensions given by Google Earth to get a rough estimate of the length around each monolith, and input it into my data table. The final Google Earth map of the monoliths was produced by overlaying a topographic map file onto Google Earth.

**4. Results & Discussion**:

*Spatial Distribution.* Twenty-nine monoliths were identified in the Swauk Watershed and mapped on the final Google Earth map. Sixteen of them were visited while thirteen were not visited but were mapped. We took measurements from about 55% of the total monolith count in the Swauk Watershed (Table 1) (Fig. 10). The majority of the monoliths were found north of Liberty, WA in topographically higher regions of the Swauk Watershed, and south of the Swauk Campground near US 97, in the Hurley Creek area. We speculate monoliths to be found in these parts of the Swauk Watershed and not others because of neighboring landslide territory to the east, the prominence of dikes to the west, and possible

differences in lithological facies to the north that might influence the distribution of the sandstone monoliths.

*Composition*. The monoliths all have distinct and traceable conglomerate layers that are highly resistant to erosion, as well as thick arkosic sandstone layers and some smaller pebble layers (Fig. 11). Grain sizes of the sandstone units range from 0.125 mm (fine sand) to 256 mm (cobble) (Table 2). The sorting of these grains were mainly poorly sorted, with variations of moderately to well sorted in smaller abundances (Table 2). Faces on monoliths LG1, CT1, CG2, BMJ1, HC2, SCG1, SCG2, SCG3 all reacted with HCl when applied. This implies that the sandstones of these monoliths contain calcium carbonate, and are actively undergoing chemical weathering in the form of carbonation.

Taylor, et al. (1987) describes the conglomerate facies of Cougar Gulch as mainly pebble to boulder conglomerate, conglomeritic sandstone, and medium to coarse-grained sandstone that is thickly bedded and crudely stratified. Peoples (1984) describes the Swauk formation as a 5000 m thick formation of non-marine strata, composed mainly of feldspathic to lithofeldspathic cross-bedded sandstone and interbedded dark carbonaceous siltstone and shale, which is less resistant to weathering than the sandstone.

*Structure.* From sites LG2 to BMJ1 and HC1 to CT1, there is a prominent NW/SE trend to the monoliths, with the exception of SCG2 to HC2, whose trends vary from a NE/SW azimuth to an E/W and N/S azimuth (Fig. 10). All monoliths studied are associated with dipping strata (Fig. 11). Dip slopes are gently sloping while anti-dip slopes are much steeper (Fig. 4). Of the 24 strike and dip measurements taken on the sandstone and conglomerate (Table 3), the majority of the bedding is oriented West-Northwest between a strike of 270-330 (Fig. 12), and the beds are gently dipping at 11-20° (Fig. 13). The maximum value for strike, which represents ~21% of the Strike & Dip data, lies between the orientations of 280-310, which is within the range expected from the histograms in Figures 12 and 13 (Fig. 14).

Comparing previous structural data with mine, it is apparent that all the strike and dip measurements I took in the field follow the alignment of the crests and troughs of the synclines and

anticlines of the area. (Fig. 15). The spatial distribution of the monoliths also align with local geologic structures, as seen from previous strike and dip measurements taken by Tabor et al. in 1982 (Fig. 15).

**Table 1.** The location of the monoliths listed in terms of GPS coordinates and elevation. Feature names provided are plotted on Fig. 10.

| Monolith Location | | | | |
|---|---|---|---|---|
| **Feature Name** | **Latitude (°N)** | **Longitude (°W)** | **Elevation (ft)** | **Field visit?** |
| LG1 | 47.29179 | 120.6606 | 3429 | yes |
| LG2 | 47.29437 | 120.66525 | 3414 | yes |
| LP1 | 47.29048 | 120.65474 | 3470 | yes |
| LP2 | 47.29048 | 120.65474 | 3470 | yes |
| LP3 | 47.29042 | 120.65608 | 3450 | yes |
| CT1 | 47.49742 | 120.64618 | 3365 | yes |
| CT2 | 47.29742 | 120.64618 | 3365 | yes |
| LR1 | 47.30107 | 120.63708 | 3795 | yes |
| CG1 | 47.27674 | 120.64193 | 3697 | yes |
| CG2 | 47.27674 | 120.64193 | 3697 | yes |
| BMJ1 | 47.28769 | 120.64866 | 3769 | yes |
| HC1 | 47.3091 | 120.65168 | 3557 | yes |
| HC2 | 47.31403 | 120.64558 | 3713 | yes |
| SCG1 | 47.32731 | 120.65292 | 3320 | yes |
| SCG2 | 47.32688 | 120.65469 | 3355 | yes |
| SCG3 | 47.32301 | 120.64708 | 3635 | yes |
| 1 | 47.30471 | 120.63497 | 4033 | no |
| 2 | 47.30458 | 120.63530 | 3971 | no |
| 3 | 47.29284 | 120.63293 | 4128 | no |
| 4 | 47.28751 | 120.64410 | 3498 | no |
| 5 | 47.28678 | 120.64375 | 3515 | no |
| 6 | 47.31695 | 120.64407 | 3618 | no |
| 7 | 47.31724 | 120.64483 | 3637 | no |
| 8 | 47.31786 | 120.64610 | 3686 | no |
| 9 | 47.32108 | 120.64598 | 3595 | no |
| 12 | 47.31254 | 120.64875 | 3637 | no |
| 14 | 47.31897 | 120.65616 | 3419 | no |
| 15 | 47.32270 | 120.67151 | 3243 | no |
| 16 | 47.32184 | 120.66979 | 3447 | no |

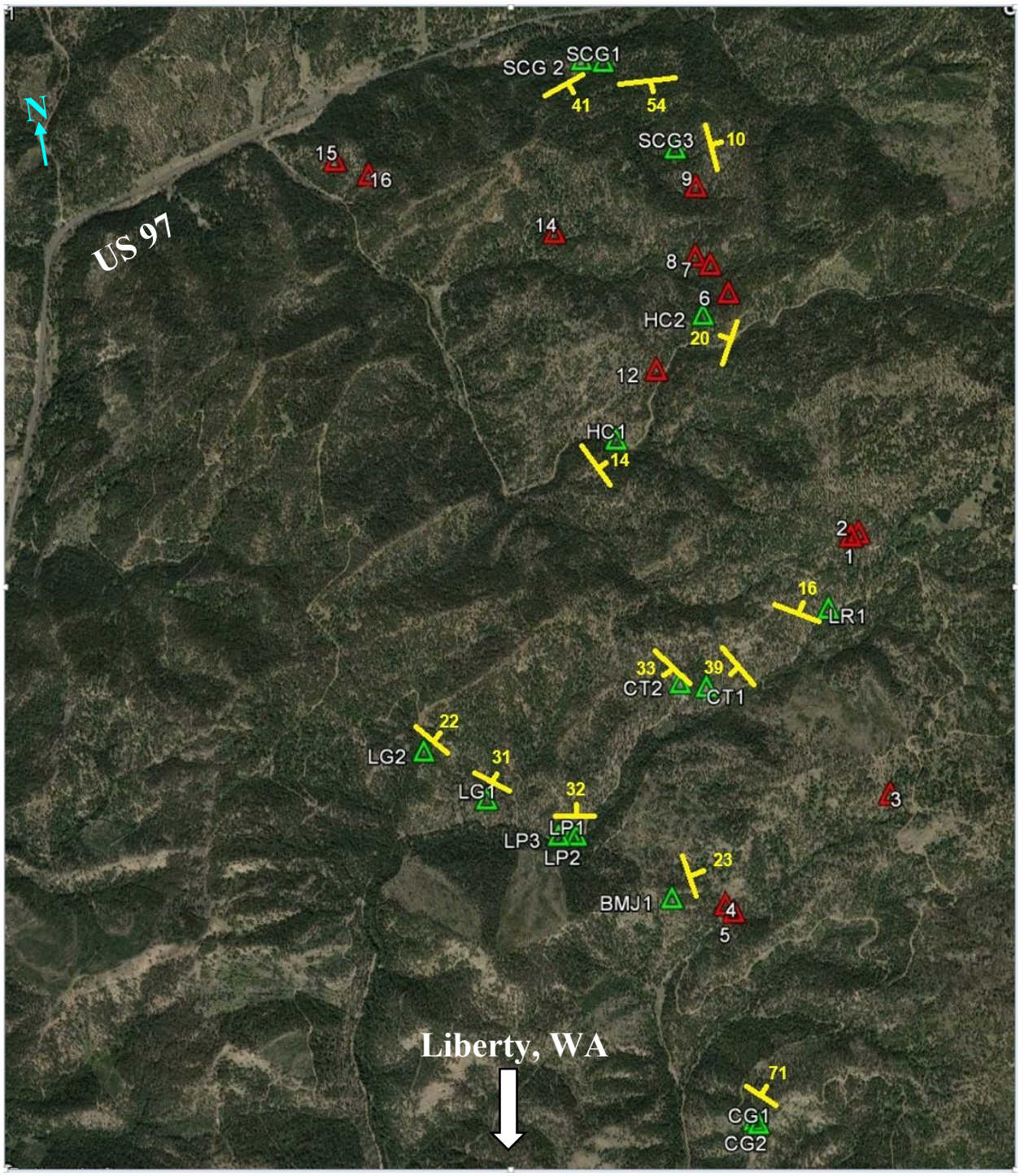


**Fig. 10**. Monoliths found near the Swauk Campground are labeled with the "SCG" series, while monoliths found near Hurley Creek are labeled with the "HC" series. All labels were designated by neighboring creeks or other meaningful features. Green triangles indicate monoliths visited. Numbered red triangles indicate monoliths mapped from Google Earth. Yellow strike and dip symbols were measured from the monoliths. Final map file can be accessed in attached CD-ROM.

**Fig. 11.** E/SE face at site LG2. Field partner Daniel O'Dell for scale. Thick sandstone unit beneath conglomerate (darker). Thin, traceable pebble layers (non-imbricated) also wrap around the sandstone.

**Table 2.** The geology of the monoliths are described in terms of grain sizes, grain sorting of beds, compositions, bedding thicknesses, as well as strike and dip. ss is the abbreviated form for sandstone; cgl is the abbreviated form for conglomerate, and mod to well sorting means the grains are moderately to well sorted.

| Geology | | | | |
|---|---|---|---|---|
| **Feature Name** | **Bedding types** | **Grain sizes** | **Sorting** | **Thickness of bedding (m)** |
| LG1 | cobbles, ss | Fine to cobbles | mod to well | ss (fine): 2-10 |
| LG2 | | med to coarse | mod to well | sand: 0.01-0.03 |
| LP1 | cobbles, ss | med to cobble | poor | massive ss |
| LP2 | ss, cgl | med to cobble | poor | ss: 0.05-0.01 |
| LP3 | | med to pebble | mod to well | ss: 5-20 |
| CT1 | ss, cgl | med to cobbles | mod to poor | ss: 1-5 |
| CT2 | sandstone | med to coarse | well | ss: <3-5 |
| LR1 | ss, cgl | coarse to cobble | well | cgl: 2 |
| CG1 | ss | coarse to cobble | poor | |
| CG2 | ss | coarse with granules | poor | 0.03-0.04 coarse lenses |
| BMJ1 | ss, cgl | fine, very convoluted | mod | massive ss above cgl |
| HC1 | ss | mod to coarse | well | 5-10 |
| HC2 | ss, cgl | med to coarse | well | ss: Height of whole thing |
| SCG1 | ss, cgl | coarse | mod to well | ss: 3.09 |
| SCG2 | ss, cgl | coarse to cobble | poor | ss: 20 |
| SCG3 | ss, cgl | med to coarse | poor | ss: 10-15 |

**Table 3.** Strike and dip measurements taken on sandstone and conglomerate bedding surfaces.

| Feature Name | Strike | Dip |
|---|---|---|
| LG1 | 300 | 31 |
| LG2 | 307 | 26 |
| LG2 | 309 | 19 |
| LG2 | 320 | 21 |
| LP1 | 339 | 20 |
| LP2 | 276 | 27 |
| LP3 | 265 | 38 |
| CT1 | 140 | 32 |
| CT1 | 145 | 42 |
| CT2 | 135 | 33 |
| LR1 | 290 | 16 |
| CG1 | 300 | 71 |
| CG2 | 300 | 71 |
| BMJ1 | 340 | 25 |
| BMJ1 | 340 | 21 |
| HC1 | 325 | 14 |
| HC2 | 200 | 20 |
| HC2 | 200 | 20 |
| HC2 | 250 | 10 |
| HC2 | 190 | 20 |
| SCG1 | 85 | 54 |
| SCG2 | 63 | 41 |
| SCG3 | 330 | 12 |
| SCG3 | 345 | 10 |

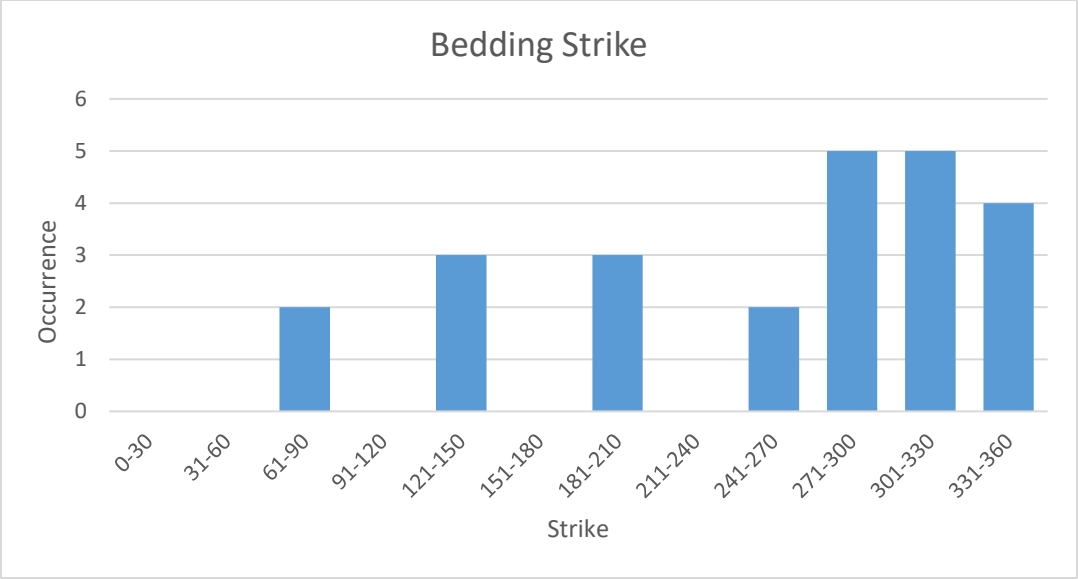


**Fig. 12.** Monolith classes described in terms of strike. The 271-300 and the 301-330 classes have the highest occurrence.

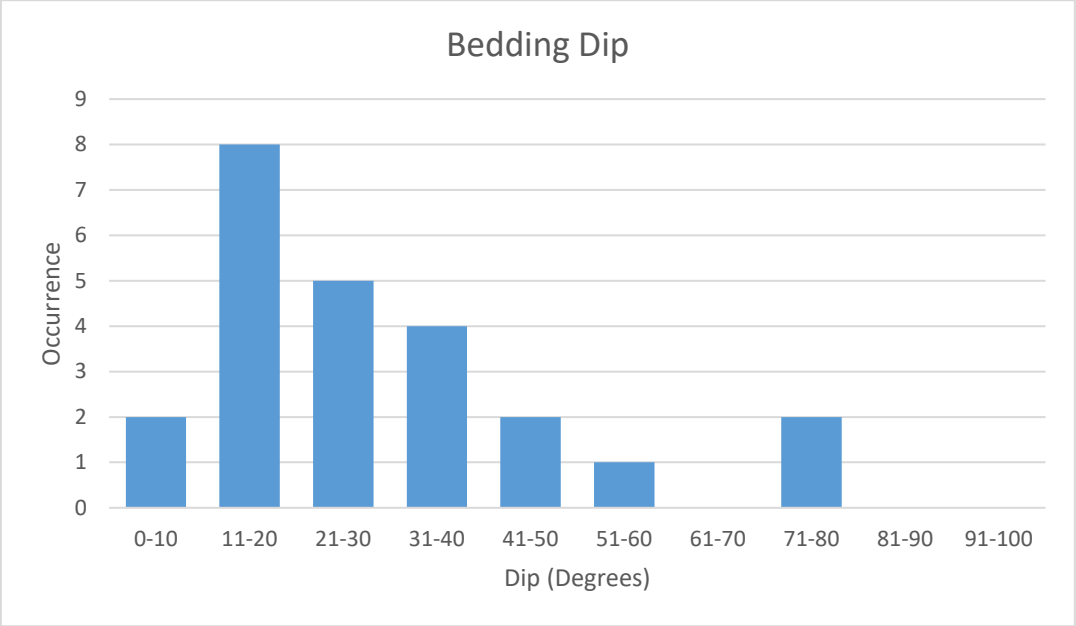


**Fig. 13.** Monolith classes described in the context of degrees dip. The 11-20 class has the highest occurrence.

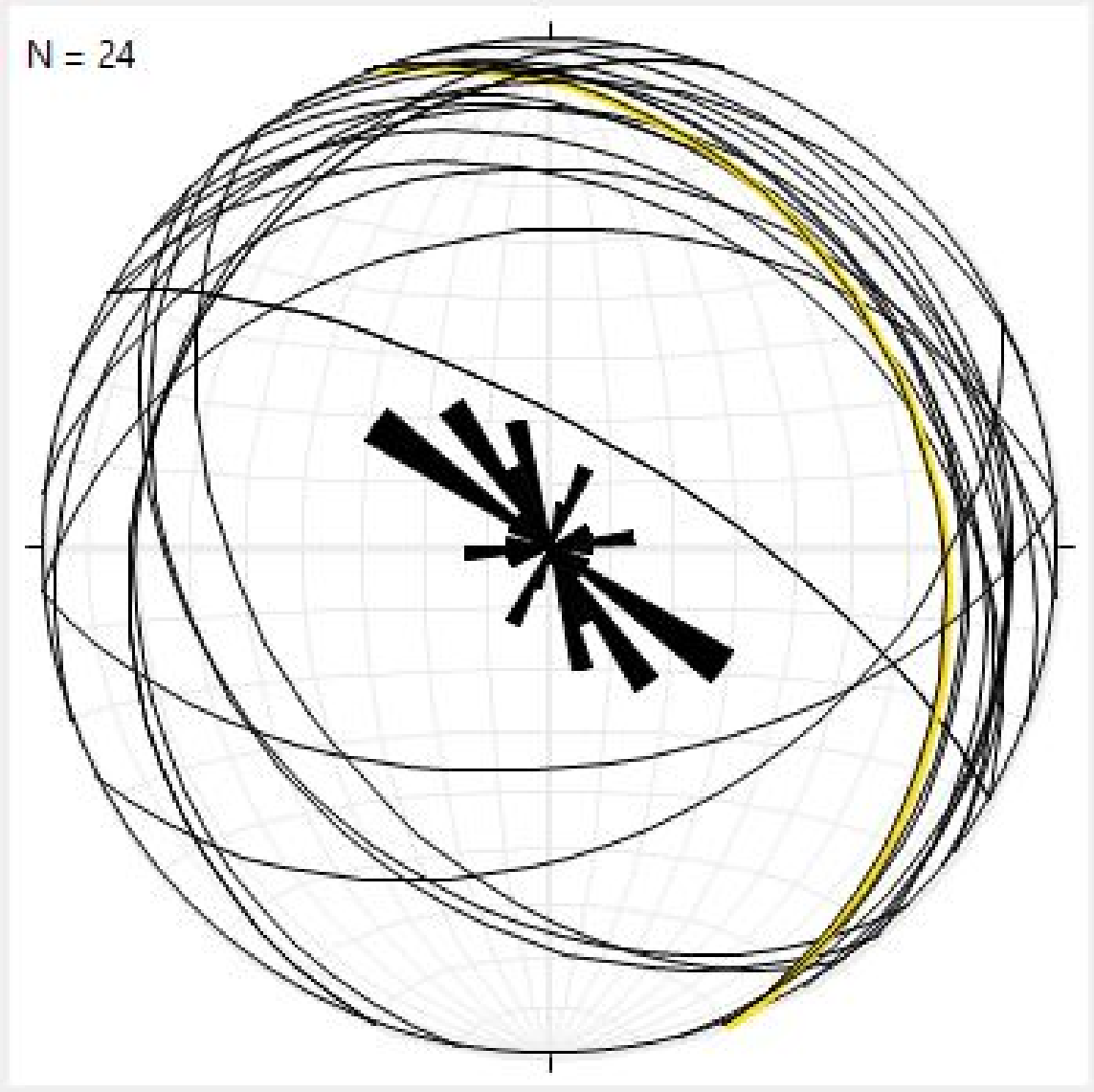


**Fig. 14.** Strike and dip measurements plotted on Stereonet 9 software as planes. Rose Diagram of data also included. Rose Diagram shows two maximum values between 90-220 and 280-310. Knowing the direction of dip, and using the right-hand rule for taking my strike measurements, 280-310 is the more reasonable.

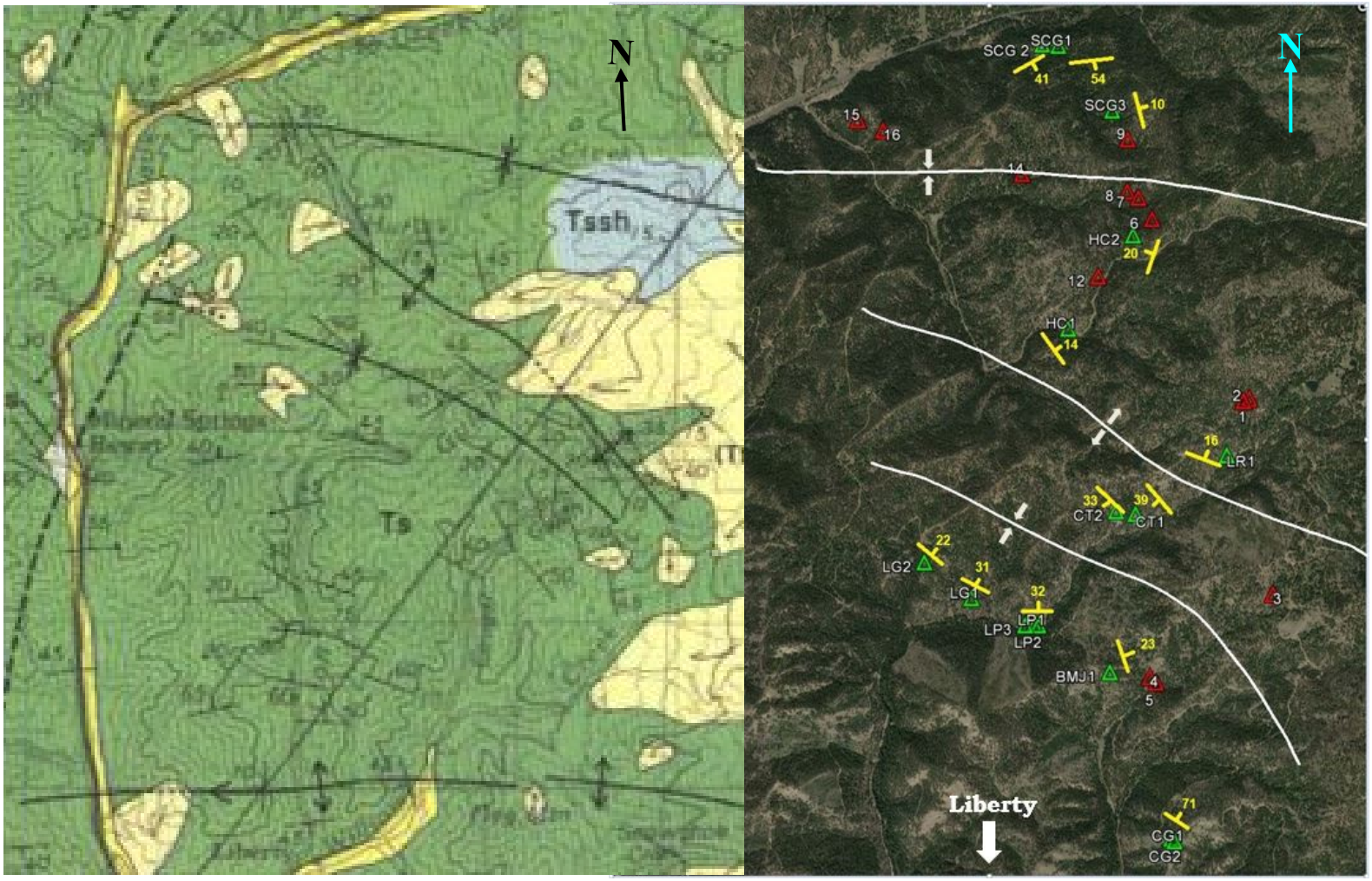


**Fig. 15.** Final Google Earth Map of monoliths in the Swauk Watershed, overlain onto Google Earth image (right) with geologic map (left) for comparison (Tabor et al., 1982). Green triangles indicate monoliths visited. Numbered red triangles indicate monoliths mapped from Google Earth. Yellow strike and dip symbols were measured from the monoliths. White lines with respective arrows indicate structural trends from Tabor et al. (1982) (left). Divergent arrows indicate a synclinal fold, convergent arrows indicate an anticlinal fold.

Lastly, joints were assessed quantitatively by measuring widths between, and gathering trend and plunge data. The width between the joints ranged from 0.02 m-20 m apart, with an average of 3.8 m (Table 4). Of the 26 trend and plunge measurements taken from the joints (Table 4), the average trend and plunge from the data is 224, 68 (Table 4).

**Table 4.** Width measurements between joints (left), and trend and plunge measurements taken from joints on the monoliths (right). Joint widths not measured are indicated by N/A.

| Joints | |
|---|---|
| **Feature Name** | **Width between (m)** |
| LG1 | N/A |
| LG2 | 0.3 |
| LP1 | N/A |
| LP2 | 0.2 |
| LP3 | N/A |
| CT1 | N/A |
| CT2 | 10-20 |
| LR1 | 0.02 |
| CG1 | N/A |
| CG2 | 0.4-0.5 |
| BMJ1 | <0.03 |
| HC1 | 0.05-0.18 |
| HC2 | 0.02-0.1 |
| SCG1 | 3 |
| SCG2 | 0.2 |
| SCG3 | 15.3 |

| Feature Name | Trend | Plunge |
|---|---|---|
| LG2 | 200 | 90 |
| LP1 | 270 | 55 |
| LP1 | 90 | 55 |
| LP2 | 170 | 90 |
| CT1 | 255 | 84 |
| CT1 | 245 | 75 |
| CT2 | 360 | 45 |
| LR1 | 290 | 16 |
| CG2 | 200 | 60 |
| BMJ1 | 10 | 90 |
| BMJ1 | 350 | 80 |
| HC1 | 183 | 69 |
| HC1 | 318 | 36 |
| HC1 | 328 | 84 |
| HC1 | 359 | 21 |
| HC2 | 260 | 95 |
| HC2 | 160 | 80 |
| HC2 | 250 | 87 |
| HC2 | 150 | 75 |
| HC2 | 255 | 87 |
| SCG1 | 135 | 77 |
| SCG2 | 305 | 35 |
| SCG2 | 295 | 42 |
| SCG2 | 230 | 62 |
| SCG3 | 105 | 80 |
| SCG3 | 55 | 90 |

The maximum value for trend, which represents ~12% of the Trend & Plunge data, lies between the orientations of 71-80 (Fig. 16). However, there are a wide variety of measurements that were taken in the field for joints (Fig. 16). Rock masses that have undergone a multitude of stresses over a period of time tend to develop more joints (Bierman and Montgomery, 2014). Our results indicate that a number different stress episodes have acted on the monoliths over time.

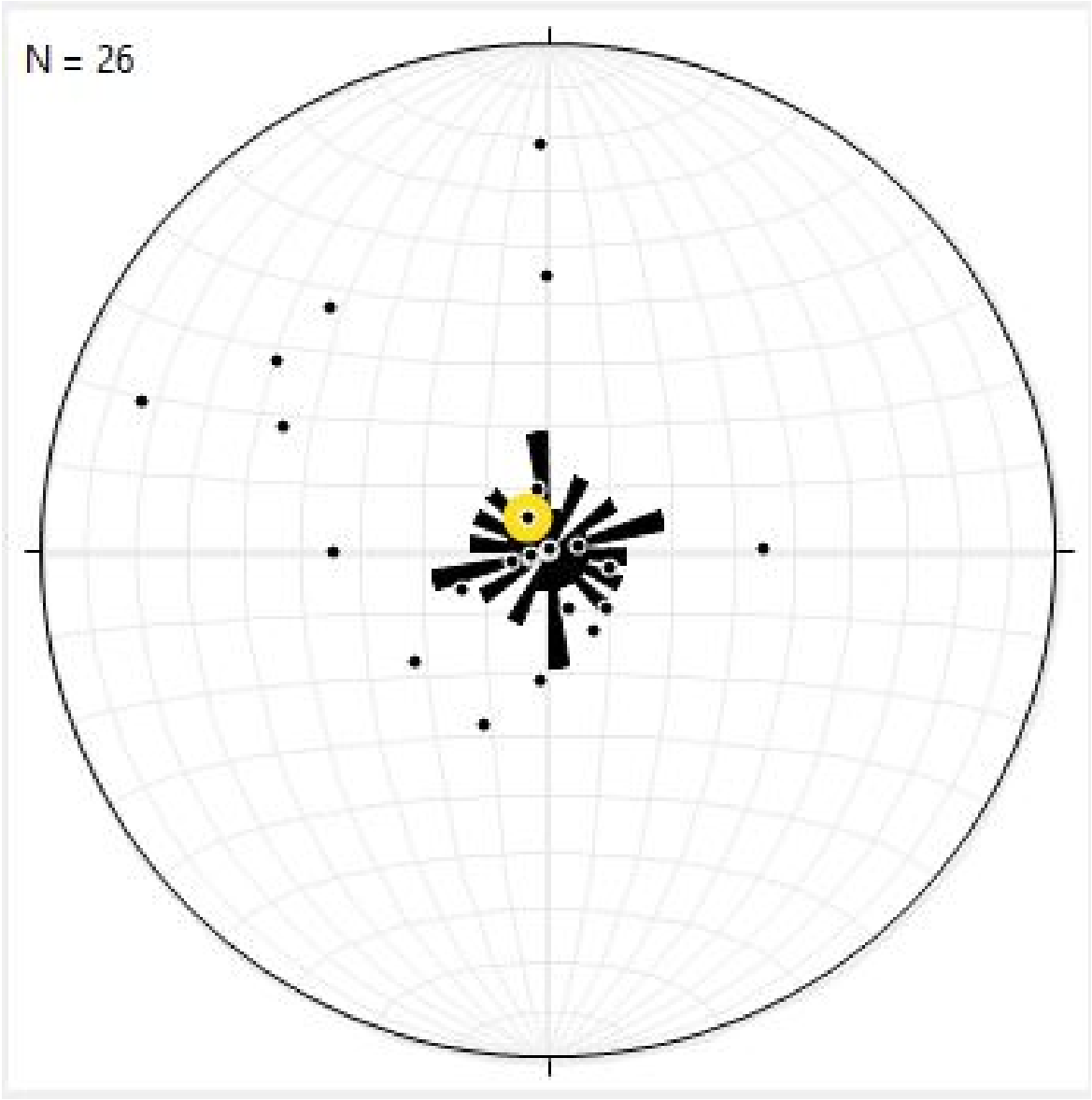


**Fig. 16.** Trend and plunge measurements plotted on Stereonet 9 software as lines. Rose Diagram of data also included. Rose Diagram shows four maximum values between 71-80, 171-179, 250-260, and 340-350. Because the variation of data is widely-distributed, the results could indicate a number of different stresses acting on the monoliths over time.

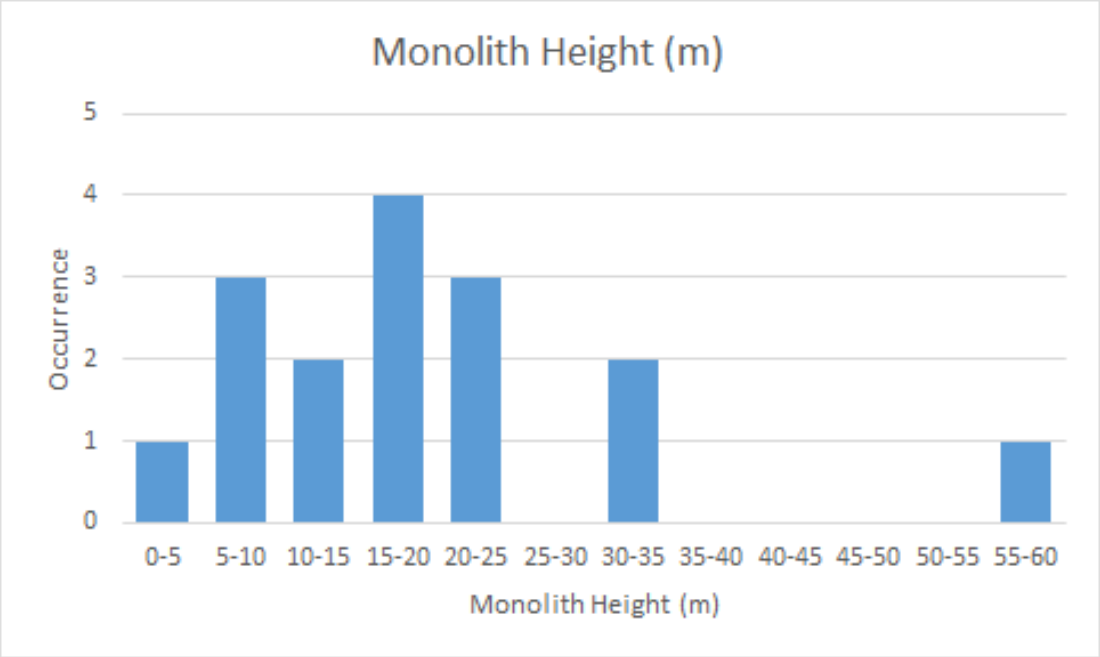


**Fig. 17.** Monoliths described in the context of height classes.

*Geomorphology.* The Swauk Watershed monoliths all share similar geomorphology: they are surrounded by channels; fresh surfaces are lichen-free; and honeycomb weathering and overhangs dominate the anti-dip slopes.

The monoliths range from 3-57 m in height, with an average of 21 m (Fig. 17) (Table 5). The monoliths range from 11-642 m in length, with an average of 182 m (Table 5). The shapes of the monoliths were either asymmetrical, cliff-like, or pillar-shaped (Figs. 18-20) (Table 5).

**Table 5.** Monolith dimensions (including length and height) and their respective shapes. Heights were calculated via Google Earth, a laser rangefinder, and the Pythagorean Theorem; Lengths around the monoliths were measured via Google Earth and the LG Health app. Shapes not observed are indicated by N/A.

| **Size and Shape** | | | |
|---|---|---|---|
| **Feature Name** | **Length (m)** | **Height (m)** | **Shape** |
| LG1 | 140 | 22.4 | Tilted, asymmetrical |
| LG2 | 94.4 | 16.6 | Pillar, asymmetrical |
| LP1 | 56.9 | 19 | Cliff-like |
| LP2 | 94.4 | 16.6 | N/A |
| LP3 | 130 | 31 | Asymmetrical & cliff-like |
| CT1 | 260 | 15.4 | Asymmetrical, tilted |
| CT2 | 365 | 14.3 | Tilted |
| LR1 | 31 | 7.2 | Asymmetrical |
| CG1 | 23 | 7 | Pillar, tilted |
| CG2 | 11 | 5.2 | Pillar and tilted |
| BMJ1 | 642 | 23.2 | Pillar, Cliff-like, tilted |
| HC1 | 231 | 11.7 | Cliff-like, asymmetrical |
| HC2 | 261 | 23.4 | Cliff-like, ridge-like, asymmetrical |
| SCG1 | 72 | 3.3 | Asymmetrical, blobby, half cone shaped |
| SCG2 | 231 | 56.7 | Pillar |
| SCG3 | 265 | 32 | Pillar |

**Fig. 18.** Example of an asymmetrical monolith. NW face of CT1. Field partner Dallin Jensen for scale. Daniel O'Dell photo.

**Fig. 19.** Example of a cliff-like monolith. NW face of LP1. Myself for scale. View from the dipping slope. The sides and other end were cliff-like. Daniel O'Dell photo.

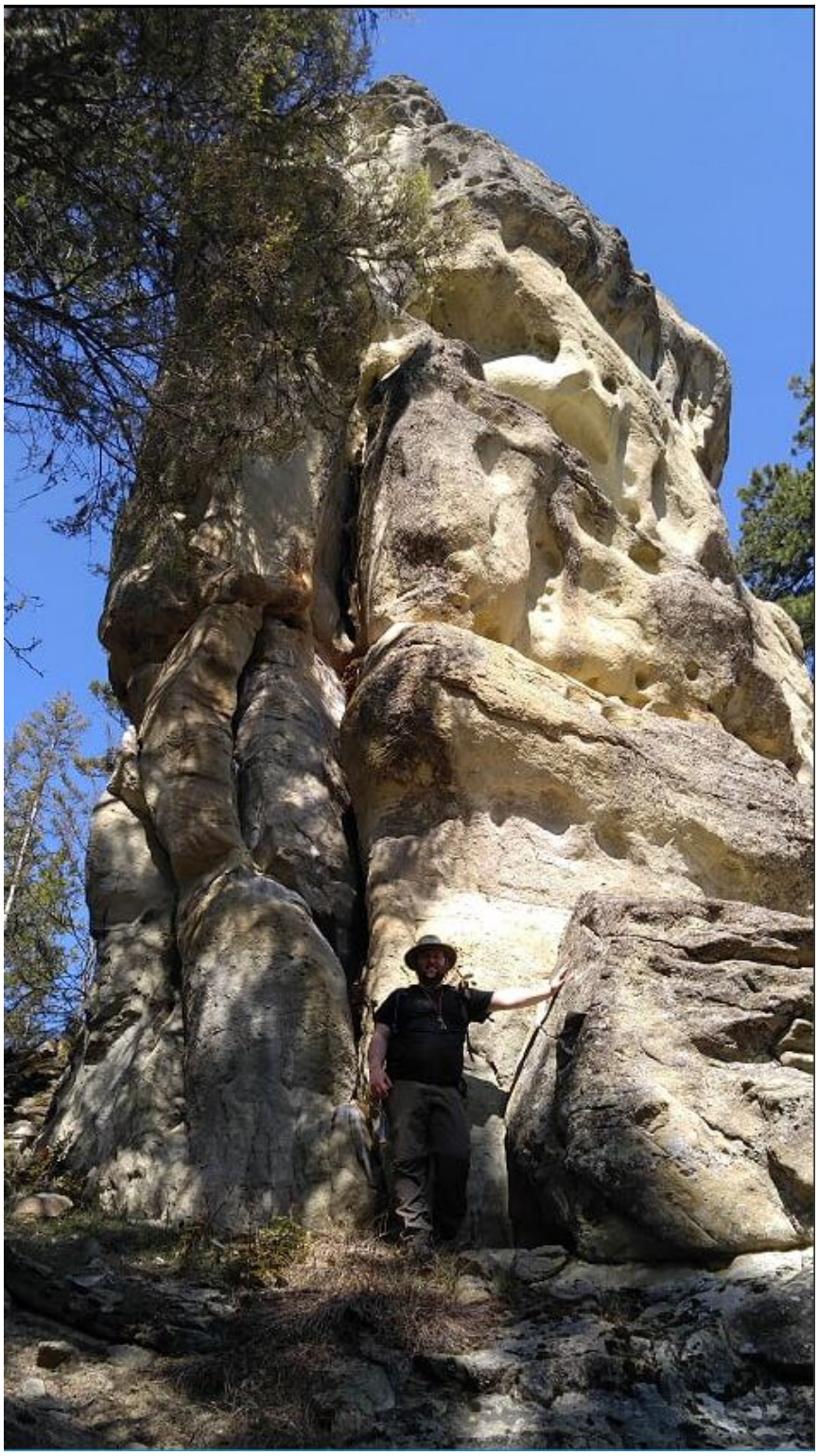

**Fig. 20.** Example of a pillar-shaped monolith. S/SW face of LG2. Field partner Daniel O'Dell for scale. Classic honeycomb weathering is visible on the upper part of the monolith. Author photo.

The aspects (i.e. orientations) of all anti-dips were also measured from all monoliths. There was a wide range of aspects that held anti-dip slopes, but the prominent aspect was between 130-210°, or on the SE-SW faces of the monoliths (Table 6) (Fig. 21).

**Table 6.** Aspects in degrees of the anti-dip slopes located on each monolith visited.

| **Aspect of Anti-dip slopes** | |
|---|---|
| **Feature Name** | **Aspect(s) (°)** |
| LG1 | 210, 290 |
| LG2 | 130, 170, 310 |
| LP1 | 145 |
| LP2 | 165, 231 |
| LP3 | 190 |
| CT1 | 105 |
| CT2 | 90 |
| LR1 | 210 |
| CG1 | 130, 210 |
| CG2 | 125, 205 |
| BMJ1 | 220 |
| HC1 | 325 |
| HC2 | 200, 250 |
| SCG1 | 325 |
| SCG2 | 50 |
| SCG3 | 180 |

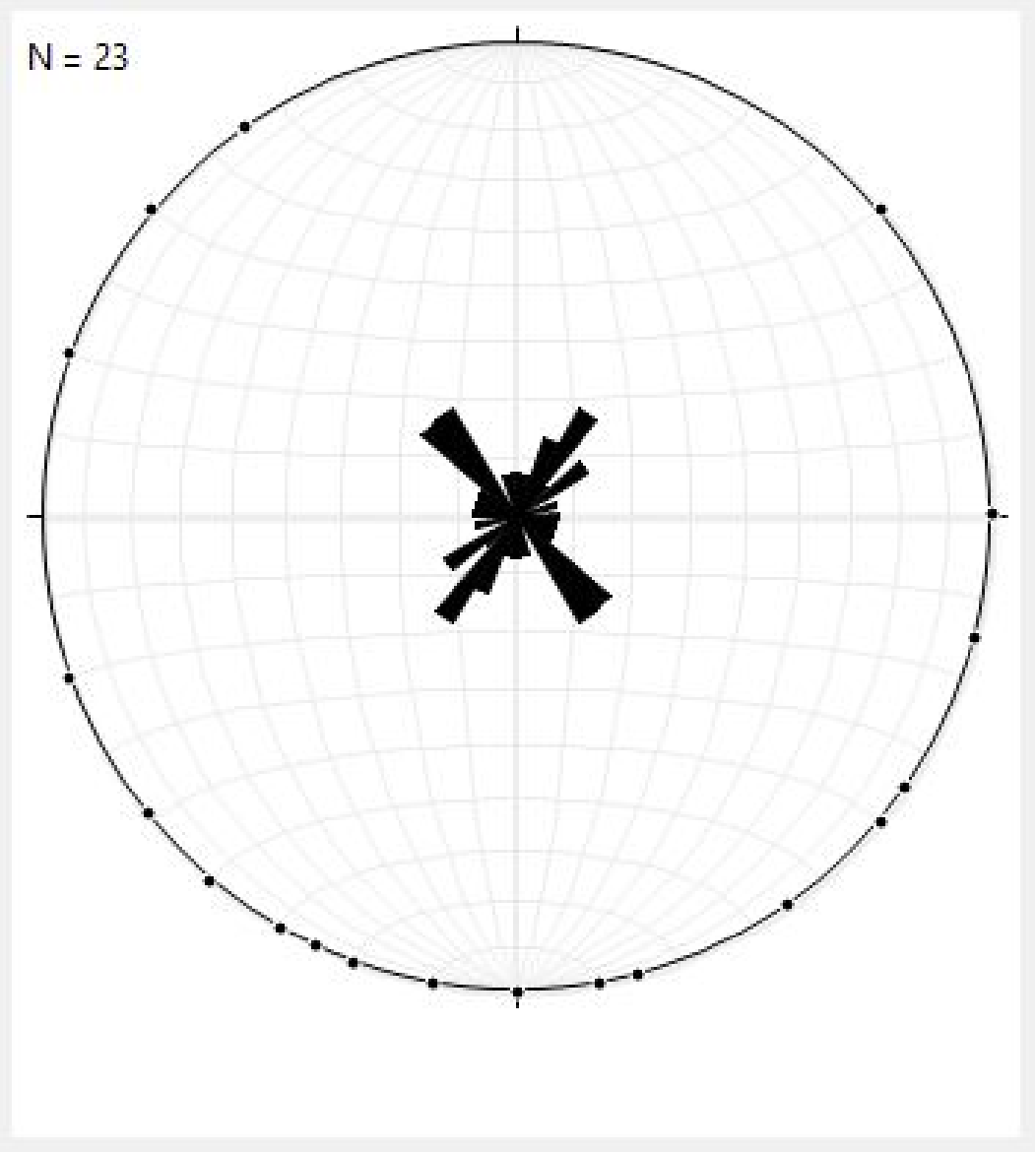


**Fig. 21.** Anti-dip aspects plotted as Rose Diagram on Stereonet 9 software. Rose Diagram shows a prominent anti-dip aspect oriented on the SE/NW face of monoliths.

Honeycombs found on the monoliths are a weathering feature that gives the monoliths a Swiss cheese-like appearance (Fig. 20) (Fig. 22). Honeycombs dominate the anti-dip slopes. These features are known in the literature as tafoni, which are defined as dissolution pits and cavities usually found on highly carbonate outcrops (Bierman and Montgomery, 2014). The 12 aspect measurements for the honeycombs average 181° (S-trending), which is within the 130-210° aspect range where the anti-dip slopes are most prominent. The sizes of the honeycombs range from 0.02-5.0 m, with an average of 0.5 m (Table 7).

**Fig. 22.** Prime example of honeycomb weathering. S face of CG2. Myself for scale. Daniel O'Dell photo.

**Table 7.** Monoliths listed under a morphological context, which includes honeycomb weathering, cannonballs, and overhangs. Cannonball sizes are averages. f*=reacts to HCl. Data not taken are indicated by N/A.

| Morphology | | | | | | | | | |
|---|---|---|---|---|---|---|---|---|---|
| Honeycombs | | | | Cannonballs | | | Overhangs | | Nearby channels ? |
| Feature Name | Aspect | Size (m) | Shape | Aspect | Size (cm) | Shape | Aspect | Diameter (m) | |
| LG1 | 210 | N/A | Oblong | N/A | 20 | N/A | N/A | 0.5-2 | No |
| LG2 | N/A | N/A | N/A | N/A | 30 | N/A | N/A | 0.5 | No |
| LP1 | N/A | N/A | N/A | N/A | N/A | N/A | N/A | 3 | N/A |
| LP2 | N/A | N/A | N/A | N/A | N/A | N/A | N/A | 1 | N/A |
| LP3 | N/A | 1-1.5 | Ellipse | N/A | 30 | Circular | N/A | 3 | Extinct |
| CT1 | 105, 220 | 1-4 | Circular | N/A | N/A | N/A | 105 | 1-1.5 | Yes |
| CT2 | 90 | 1-5 | Ellipse | 90 | 50 | Ellipse | 90 | 3-4 | Yes |
| LR1 | 210 | 0.1-0.2 | Oblong | N/A | 20 | N/A | N/A | N/A | No |
| CG1 | 130, 210 | 0.2-0.7 | Oblong | 210 | 8.5 | Round | 210 | 0.5-1 | No |
| CG2 | 115, 205 | 0.1-0.8 | Round | 205, 325 | 4.5 | Round | 325 | 1 | No |
| BMJ1 | 220 | 0.6-2.2 | Oblong | N/A | 30 | N/A | 325 | N/A | Yes |
| HC1 | N/A | N/A | N/A | 325 | 30 | Ellipse | 60, 170 | 2 | No |
| HC2 | 250 | 0.02-0.2 | Egg | 250, 170 | 40 | Oblong | 300, 325 | 3-5 | No |
| SCG1 | N/A | N/A | N/A | 175 | 25 | Round | 270 | 0.7-7 | Yes |
| SCG2 | N/A | N/A | N/A | 270, f* | 29.5 | Ellipse | 200, 30 | 4 | Yes |
| SCG3 | 210 | <1-5 | Egg | 320, 210 | 43 | N/A | N/A | 3-25 | Yes |

Cannonballs occur mostly on the west faces of the monoliths, and, of the 11 aspect measurements, their average aspect was 232° (S/SW-trending) (Table 7). These rounded to ellipsoid-shaped features are embedded into the sandstone, and all of them react with HCl when applied (Figs. 5, 6, and 7). The sizes of the cannonballs range from 4.5-50 cm across, with an average of 28 cm (Table 7). These cannonballs are also known as cannonball concretions, or nodules, and are often perfectly spherical. They form by the selective precipitation from ground water of dissolved minerals, most commonly calcium carbonate (Biek, 2002), which explains their reactivity with HCl.

Monolith overhangs are mostly located on the south sides of the monoliths, where anti-dips are most prominent (Table 6). With an average aspect of 201° (S/SW-trending) (Table 7), it is also within the 130-210° aspect range for anti-dip slopes (Table 6). Overhang diameter ranged from 0.5-7.0 m (Table 7). Overhangs appear sheet-like and occur in parts of the monolith that have the most jointing (Figs. 8 and 9).

Potholes and weathering pits, though not prominent features, also occur on anti-dip slopes and monolith tops (Fig 23). Potholes are cylindrical forms eroded into rock by rapidly moving vortices carrying abrasive, sand-sized sediment (Bierman and Montgomery, 2014). Weathering pits originate in slight depressions where water gathers after rainfall or snowmelt. Whereas the surrounding surfaces soon dry out, the depression is kept moist or supports a shallow pool for long periods. The presence of water provides a locus for more rapid weathering and the depression is widened and deepened (Goudie and Migon, 1997). These weathering phenomena only occur at sites CG1, HC1, and BMJ1.

Weathered material was also found from the monoliths that blanketed surrounding slopes of the monoliths. This weathered material can be recognized as grus (i.e., coarse sand and fine gravel-sized debris) or regolith (i.e., unconsolidated rocky material), and is an accumulation of coarse-grained fragments that came from the monolith (Figs. 24, 25, and 26).

Vegetation, which consists of trees, shrubs, and herbs within 10 feet of the monolith, thrives on all monolith dip slopes. The highest % cover of biota is found at sites SCG2 and CT2 (Table 8).

**Fig. 23.** W face of site CT2 showing weathering pits on the dipping slope of this asymmetrical monolith. Author photo.

.

**Fig. 24.** Typical sandy grus found among dirt and soil. E face of LR1. Field partner Dallin Jensen for scale. Author photo.

**Fig. 25.** Typical rocky regolith showing weathering downhill in large fragments. Field partner Dallin Jensen and myself for scale. Site HC1. View SW. Daniel O'Dell photo.

**Fig. 26.** NE face of BMJ1 with a combination of weathered regolith and grus on the ground. Field partner Daniel O'Dell for scale. Author photo.

**Table 8.** Monoliths are grouped by biota, which mainly includes shrubbery, herbs, and other alike foliage surrounding the features. % cover not measured indicated by N/A.

| Biota | | | |
|---|---|---|---|
| **Vegetation (within 10 ft)** | | | |
| **Feature Name** | **General Types** | **% Cover** | **Are trees found on dip slopes?** |
| CT1 | Shrubs, trees | N/A | Yes |
| CT2 | Herbs, shrubs, trees | 90 | Yes |
| LR1 | Herbs | 60 | Yes |
| CG1 | Herbs, shrubs, trees | 80 | Yes |
| CG2 | Herbs shrubs trees | 80 | Yes |
| BMJ1 | Herbs, shrubs, trees | 85 | Yes |
| HC1 | Herbs, shrubs, trees | 60 | Yes, in fewer amounts on dip slope |
| HC2 | Herbs, shrubs, trees | 80 | Yes |
| SCG1 | Herbs, shrubs, trees | 65 | Yes, all around |
| SCG2 | Herbs, shrubs, trees | 90 | Yes |
| SCG3 | Herbs, shrubs, trees | N/A | Yes |

Though vegetation is found along all aspects of the monoliths, the dip slopes have the highest concentration of trees, with about 100% coverage at site SCG2 (Table 8). Out of 15 aspect measurements of lichen found on the monoliths, the average is 168° (S/SE-trending), which also corresponds with the aspects of prominent anti-dip surfaces.

Lichen growth covered the most area at sites SCG1 and SCG2 (Table 9) (Fig. 27). We also noticed that no lichen growth occurred on anti-dip surfaces, implying that these monoliths are still actively being weathered on anti-dip slopes. The areas with the most lichen coverage correspond with the areas of most stability but are not actively being eroded away.

**Table 9.** A continuation from Table 7 showing lichen coverage and vegetation location among monolith surfaces. Data not recorded indicated by N/A.

| Biota Continued | | | | |
|---|---|---|---|---|
| Vegetation (within 10 ft) | | Lichen Coverage | | Notes |
| Feature Name | Where vegetation is mostly located? | % | Aspect | |
| LG1 | N/A | 50 | 210 | N/A |
| LG2 | N/A | 80 | N/A | N/A |
| LP1 | N/A | 50 | N/A | N/A |
| LP2 | N/A | 45 | N/A | N/A |
| LP3 | N/A | 50 | N/A | N/A |
| CT1 | Dip slope | 15 | 105 | N/A |
| CT2 | Dip slope | 10 | 90 | N/A |
| LR1 | Dip slope | 50 | N/A | N/A |
| CG1 | Same amount everywhere | 80 | N/A | N/A |
| CG2 | Same amount everywhere | 40 | N/A | N/A |
| BMJ1 | Same amount everywhere | 60 | N/A | cgl: 85% ss: 20% |
| HC1 | Sides | 80 | 300 | N/A |
| HC2 | Same amount everywhere | 65 | 60 | N/A |
| SCG1 | Sides | 90 | 325 | N/A |
| SCG1 | N/A | 95 | 196 | N/A |
| SCG1 | N/A | 40 | 300 | N/A |
| SCG2 | Dip slope | 90 | 50 | N/A |
| SCG2 | N/A | 30 | 270 | N/A |
| SCG2 | N/A | 100 | 395 | N/A |
| SCG3 | N/A | 30 | 320 | More lichen located closer to the ground |
| SCG3 | N/A | 10 | 30 | |
| SCG3 | N/A | 10 | 180 | N/A |
| SCG3 | N/A | 99 | 10 | N/A |

**Fig. 27.** Lichen (dark brown and green spots) seen on the E face of CT1. Author photo. Full compilation of field data can be accessed via the attached CD-ROM.

**4. Interpretation**:

After having observed that the monoliths are all related structurally, compositionally, and geomorphically, these results indicate that geologic structure and composition play a significant role in the initial shaping of these landforms. Differential weathering, fluvial erosion, and mass movement weakened the sandstone to cause low bedrock escarpments to retreat on the slopes, which carved out vertically aligned joints. It had to have been the repetitive cycle of weathering, mass movement, and stream erosion has ultimately been the cause of the isolation of the sandstone monoliths over time. In order to better understand the formation of the monoliths, an origins model was created below:

1. Deposition. W to SW flowing streams laid down sands and gravels of the Swauk formation (Eddy et al., 2015). Evidence: sedimentary structures, and cannonballs.
2. Lithification. Evidence: different rock units.

3. First generation folding (E/NE trending) originated in the central portion of the Swauk Watershed (Doran, 2009). Evidence: tilted strata.
4. Intrusion by Teanaway dikes (Miller, 2014) recorded a counterclockwise extensional event (Doran, 2009). Evidence: linear ridges of NE-trending basalt cutting the Swauk Formation (Doran, 2009).
5. Second generation folding (NW trending) further complicate geology. Evidence: jointing and tectonically influenced drainage reorganizations (Miller, 2014).
6. Fluvial erosion I. Evidence: extinct channels, homoclinal ridges, asymmetrical monoliths, and potholes on the anti-dip slopes.
7. Fluvial erosion II. Evidence: Monolith backwasting, pillar and cliff-like shapes, and overhangs. The eroded and isolated products are called flatirons (i.e., steeply sloping triangular facets).
8. Weathering (Hydrolysis, Exfoliation, Carbonation and Frost action). Evidence: grus, honeycombs and weathering pits, and cannonballs that react to HCl.
9. Mass Movement. Evidence: removal of grus; rockfall from the anti-dip surfaces & sides.

**5. Conclusions & Future Research**:

Although these features have been explained as products of either subsurface water erosion and selective weathering (Alexandrowicz and Urban, 2005), or differential weathering and mass movement (Dyke, 1976), our field investigations support a combination of all the above processes. A series of tectonic uplift of sandstone and conglomerate, mass movement, weathering, fluvial erosion, and backwasting have together influenced the genesis of the monoliths in the Swauk Watershed.

There is no doubt in our minds that the monoliths are tors, as they match the definitive criteria: they are individual rocky features that form separated from the slope and other landforms, and are characterized by walls sculpted primarily by weathering processes.

To further sort out these monoliths, future researchers could study the sedimentology and stratigraphy of the twenty-nine features we mapped in order to assign them to a particular facies within

the Swauk Formation as well as understand what is controlling the distribution of these monoliths under the context of Swauk Basin sedimentology.

In the future, our data can be applied to adjacent Peshastin Creek and Teanaway River watersheds in order to construct a regional map of the monoliths. Further, future researchers can see how the origins of these monoliths are related to others in surrounding basins.

**6. References**:


Alexandrowicz, Z., & Urban, J. (2005). Sandstone regions of Poland Geomorphological types, scientific importance and problems of protection. *Ferrantia,* 137- 142.

Bierman, P. and Montgomery, D. (2014). Key Concepts in Geomorphology. *A. Macmillan Higher Education Company.* Text.

Biek, N. (2002). "Concretions and Nodules in North Dakota." *North Dakota Geological Survey.* Web. https://www.dmr.nd.gov/ndgs/ndnotes/concretions/concretions.asp

Camp, A. E. (1999). Age Structure and Species Composition Changes Resulting from Altered Disturbance Regimes on the Eastern Slopes of the Cascade Range, Washington. *Journal of Sustainable Forestry*, 9. 39-67.

Doran, B. (2009). Structure of the Swauk formation and Teanaway dike swarm, Washington Cascades. *Masters Theses*. Paper 3717. http://scholarworks.sjsu.edu/etd_theses/3713.

Dyke, A. S. 1976. Tors and associated weathering phenomena, Somerset Island, District of Franklin. *Geological Survey of Canada*, 209-216.

Eddy, M., Bowring, S., Umhoefer, P., Miller, R., McLean, N., and Donaghy, E. (2015). High-resolution temporal and stratigraphic record of Siletzia's accretion and triple junction migration from nonmarine sedimentary basins in central and western Washington. Geological Society of America Bulletin. doi:10.1130/B31335.

Engstrom, Wesley C. (2006) "Swauk Basin History: Gold Created A Community." *Swauk Basin Wildfire Protection Plan*: 36. Web. 12 May. 2016.

Erickson, J. (2001). Historic Land Use Change in the Swauk Watershed, Central Washington. *Central Washington University.* 1-29.

Evans, J. (1994). Depositional History of the Eocene CHumstick formation- Implications of Tectonic Partitioning for the History of the Leavenworth and Entiat-Eagle Creek Fault Systems, Washington. *Earth, Environment, and Society Faculty Publications.* Paper 5. http://scholarworks.bgsu.edu/sees_pub/5

Goudie, A. and Migon, P. (1997). Weathering pits in the Spitzkoppe area, Central Namib Desert. *Zeitschrift fur Geomorphologie*, 41: 417-444.

Johnson, S. (1985). Eocene strike-slip faulting and nonmarine basin formation in Washington. *In* Strike-slip deformation, basin deformation, and sedimentation. *Edited by* K.T. Biddle and N. Christie-Blick. *Society of Economic Paleontologists and Mineralogists*, Special Publication 37, pp. 283-302.

Lillquist, K. (2001). "Mass Wasting in the Swauk Watershed, Washington." *Physical Geography*: 22, 3. 237-253.

Miller, Robert M. (2014). "Linking deep and shallow crustal processes in an exhumed continental arc, North Cascades, Washington." *Geological Society of America*. doi: 10.1130/2009.fl d015(19): 373-406.

Peoples, D. (1984). Sedimentology and Petrography of the Swauk Formation: Blewett Pass Area, Washington. *Masters Theses.*

Stephenson, C. (1997). "Swauk Watershed Analysis." *Cle Elum Ranger District: Wenatchee National Forest.* p. 4-23.

Tabor, R., Waitt, R. Jr., Frizzell, V. Jr., Swanson, D., Byerly, G., and Bentley, R. (1982). Geologic Map of the Wenatchee 1:100,000 Quadrangle, Central Washington. May 2016.

Taylor, S., Johnson, S., Fraser, G., and Roberts, J. (1987). Sedimentation and tectonics of the lower and middle Eocene Swauk Formation in eastern Swauk Basin, central Cascades, central Washington. *Department of Geology, University of New Mexico,* 25: 1020-1036.

**7. Acknowledgements**:

This project was funded by both the C. Farrell Fine Arts and Research Scholarship and the Office of Undergraduate Research (OUR) Grant and represents independent research by the author, under the supervision of Dr. Karl Lillquist of the Geography Department.

I wish to give special thanks to Dr. Karl Lillquist for all his advice and encouragement throughout this project, and I am grateful in his role throughout the scholarship and grant writing process. His efforts mean a lot to me personally and I am glad to have come across him as a professor and research mentor.

Special thanks are also given to Daniel O'Dell for assistance in all aspects of project in proposal, fieldwork, data analysis, and writing. I am appreciative of his eagerness in participating in my adventures every weekend, as well as his diligence in acting as the "rover" to venture to the more dangerous cliff-sides of the monoliths in order to obtain more data for this project.

I would also like to acknowledge Dallin Jensen, who took the time out of his busy schedule to join me in the field a few times to offer his advice for field methods.

Lastly, I thank Dr. Breanyn MacInnes for initiating interest in the sedimentology of the Swauk formation from her Advanced Sedimentology class in the fall of 2015.